Inhibitor selectivity: profiling and prediction

Janssen, A.P.A.

I had nothing to offer anybody but my own confusion.
Jack Kerouac

4 Structure Kinetics Relationships for irreversible DAGL inhibitors

Introduction

The last decade has seen a renewed interest in the development of covalent inhibitors for several classes of drug targets, including the serine hydrolase and kinase superfamily.[1,2] Serine hydrolases perform a broad array of physiological functions and have diverse substrate preferences, but they all share a conserved catalytic nucleophilic serine residue. Serine hydrolases form a covalent acyl-enzyme intermediate, which can be exploited by irreversible, mechanism-based inhibitors. For example, PF-04457845 and ABX-1431 have entered clinical trials as fatty acid amide hydrolase (FAAH) and monoacylglycerol lipase

(MAGL) inhibitors for the treatment of neurological diseases, respectively.[3–8] Covalent, irreversible inhibitors initially bind in a reversible fashion to the protein (i.e. the Michealis-Menten complex) followed by a time-dependent chemical reaction that inactivates the enzyme (Figure 4.1A and 4.1B).[9] The half maximum inhibitory concentration (IC_{50}) for covalent inhibitors is dependent on a combination of binding affinity (K_i) and reactivity (k_{inact}). This fundamental dual aspect of covalent inhibition is often not taken into account during the optimization of covalent irreversible inhibitors, which is usually based on IC_{50} values.[2,10] This may lead to the prioritization of highly reactive molecules (large k_{inact}) based on their high potency.[11] Intrinsic high reactivity may, however, lead to a-specific binding to other members of the same enzyme family and unwanted adverse side effects as recently witnessed for BIA 10-2474 (Chapter 5).[12,13] Of note, the specificity constant $\left(\frac{k_{inact}}{K_i}\right)$ is sometimes employed to guide inhibitor optimization to avoid IC_{50}-values that are assay- and time-dependent.[14–16] The specificity constant is determined by measuring the observed rate constants (k_{obs}) using various inhibitor pre-incubation times, but does not allow the independent optimization of the affinity K_i, while minimizing the reactivity k_{inact}. Thus, alternative methods are required to determine K_i and k_{inact} in an independent manner.

Diacylglycerol lipases (DAGL) are serine hydrolases responsible for the synthesis of the endocannabinoid 2-arachidonoylglycerol (2-AG).[17] Modulation of DAGL activity holds therapeutic promise for the treatment of metabolic and neuroinflammatory diseases.[18–20] Several DAGL inhibitors, including KT109, DH376 and LEI105, have been developed (Figure 4.1C).[20–22] KT109 and DH376 belong to the class of triazole urea inhibitors, which are capable of irreversibly binding the catalytic serine through the formation of a stable carbamate adduct, thereby expelling a triazole-moiety as a leaving group (Figure 4.1A). This class of compounds has also shown merit as inhibitors for other serine hydrolases, such as α/β-hydrolase domain containing protein (ABHD) 6[21], ABHD11[23], DDHD domain-containing protein 2 (DDHD2)[24] and MAGL[11,25]. Structure activity studies of the DAGL (KT109 and DH376) and MAGL (JJKK-048) inhibitors have shown that the heterocyclic leaving group is crucially important for inhibitor activity.[11,26,27] The pK_a of the leaving group as determinant for the reactivity of the urea[28] was postulated to determine the activity of inhibitors.[11] The exact kinetic parameters of binding for these inhibitors have, however, thus far not been experimentally measured, thus the precise role of the triazole heterocycle in the inhibitor activity is unknown.

Here, we studied in detail the influence of the heterocycle in DAGL-α inhibitor DH376 on the binding and reactivity. To this end, we synthesized a coherent set of azole derivatives of DH376 to systematically investigate the role of the heterocycle in the activity of the inhibitor. Furthermore, we adapted a surrogate substrate assay of DAGL-α, which allowed us to independently measure K_i and k_{inact} of the new inhibitors. Surprisingly, we found that the azole has a crucial role in the formation of the Michaelis-Menten complex, rather than in modulating the reactivity.

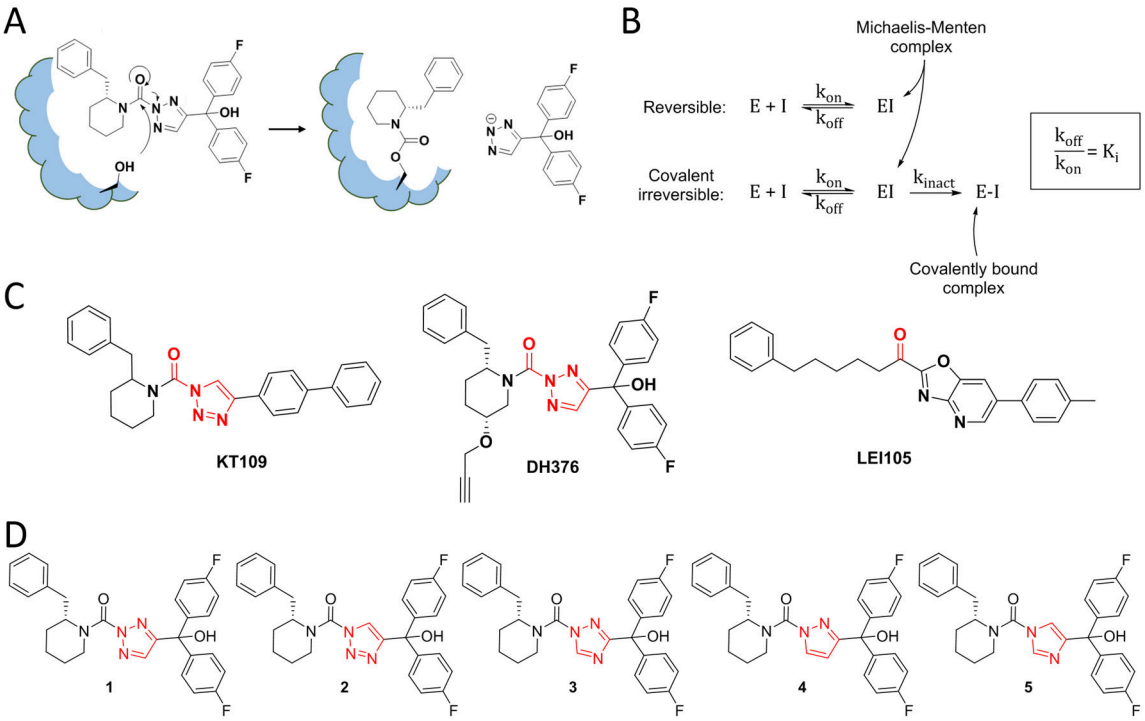

Figure 4.1 | A) Mechanism of action of mechanism based triazole urea inhibitors for serine hydrolases. B) The inhibition reactions for reversible and irreversible inhibition. E: enzyme, I: inhibitor, EI: Michaelis-Menten complex of E and I, E-I: covalently bound inhibitor-enzyme complex. C) Recently published potent DAGL inhibitors. D) Set of 5 inhibitors based on DH376 synthesized and characterized in this study.

Results

To study the role of the azole heterocycle in the activity of the DAGL inhibitor DH376, a focused set of DH376 analogues was synthesized (**1-5**) (Figure 4.1D). Four different heterocycles (1,2,3-triazole, 1,2,4-triazole, pyrazole and imidazole) and a regio-isomer were selected, because they differ five orders of magnitude in pK_a.[29–31] The compounds were synthesized according to Scheme 4.1. The enantioselective synthetic route towards (*R*)-2-benzylpiperidine was adapted from Deng *et al.*[27] We replaced the low yielding transamination step, used to introduce an alkene at the free amine of **10**, by a simple alkylation with 4-bromobut-1-ene after nosyl protection of the amine (Scheme 4.1). This protected diene was subjected to ring-closing metathesis and, after deprotection, yielded **15** in a three-fold higher overall yield than previously reported.[27] To synthesize the leaving group azole derivatives, a general synthetic route was devised featuring a Grignard reaction as core transformation to yield the di-(*p*-fluorophenyl)methanol moiety in a single step from accessible azole esters (Scheme 4.1). For all but the imidazole derivative this worked without the introduction of any protecting group. Tritylation of the imidazole ethyl ester was necessary to avoid degradation during the Grignard reaction. Finally, the secondary amine **15** was first transformed in a carbamoyl chloride using triphosgene and subsequently reacted with the diphenyl azoles (**18, 21, 25** and **29**), which furnished the inhibitors **1-5**.

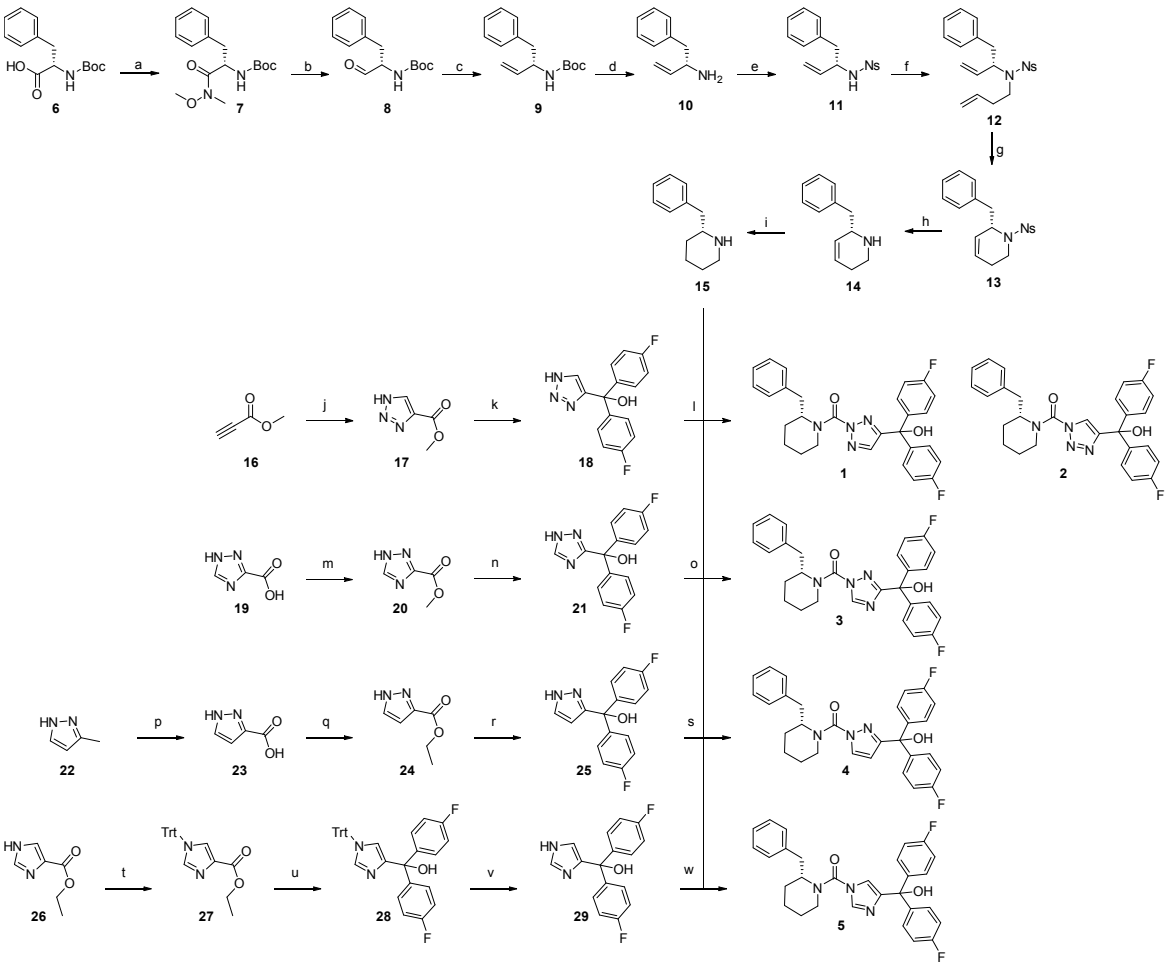

Scheme 4.1 | Synthesis of **1-5** implementing the optimized 9-step procedure for the synthesis of (*R*)-2-benzylpiperidine **15** from commercially available *N*-Boc-L-phenylalanine (**6**), followed by the coupling to the biphenyl-azole leaving groups synthesized using a general Grignard reaction. a) N,O-di-Me-hydroxylamine·HCl, EDCI·HCl, DCM, 0 °C → RT, 92%; b) $LiAlH_4$, THF, -20 °C, 96%; c) $MeP(Ph)_3Br$, KHMDS, THF, -78 °C → RT, 56%; d) HCl, MeOH/H_2O, quant.; e) NsCl, NEt_3, DMAP, DCM, 85%; f) 4-bromobut-1-ene, K_2CO_3, DMF, 70 °C, 80%; g) Grubbs' 1st gen., DCM, 40 °C, 62%; h) PhSH, NaOH, ACN/H_2O, 50 °C, 99%; i) $RuCl_3(H_2O)_3$, $NaBH_4$, DCE/MeOH, 87%; j) TMS-N_3, 90 °C, 68%; k) 4-F-PhMgBr, THF, 0 °C, 94%; l) *i*) **15**, triphosgene, Na_2CO_3, DCM; *ii*) **18**, DIPEA, DMAP, THF, 66 °C, 1.5% (**1**) 1.2% (**2**); m) MeOH, $SOCl_2$, 65 °C, 97%; n) 4-F-PhMgBr, THF, 0 °C, 89%; o) *i*) **15**, triphosgene, Na_2CO_3, DCM; *ii*) **21**, DIPEA, DMAP, THF, 66 °C, 35%; p) $KMnO_4$, H_2O, 100 °C; q) H_2SO_4, EtOH, 78 °C, 47% (two steps); r) 4-F-PhMgBr, THF, 0 °C, 83%; s) *i*) **15**, triphosgene, Na_2CO_3, DCM; *ii*) **25**, DIPEA, DMAP, THF, 66 °C, 21%; t) TrtCl, TEA, DCM, 0 °C → RT, 97%; u) 4-F-PhMgBr, THF, 0 °C, 86%; v) TFA, H_2O, DCM, 56%; w) *i*) **15**, triphosgene, Na_2CO_3, DCM; *ii*) **29**, DIPEA, DMAP, THF, 66 °C, 27%.

To determine the binding kinetics of the inhibitors we adapted the previously reported para-nitrophenolbutyrate (PNPB) assay.[32] The typical pre-incubation step with the inhibitors was omitted and enzyme activity was continuously measured from the start (t = 0). To obtain a higher specific signal at early time points, the substrate concentration was increased to 600 µM. Furthermore, the enzyme was pre-mixed with the assay buffer before addition to a 96-well plate, which contained concentrated inhibitor and substrate, to minimize initial mixing effects. This yielded reproducible substrate conversion curves (Figure 4.2).

Most available literature models, including the standard observed rate approximation (k_{obs}), assume that the enzyme concentration will not change during the incubation

(K_i >> [E]).[14,33–35] These models can, however, not be applied to potent inhibitors, such as KT109 and DH376, that will decrease the enzyme concentration. Therefore, the kinetic model of Schwartz *et al*. was selected to fit to the substrate conversion curves.[10] In this model, DynaFit software is used for the numerical fitting of the full set of differential equations governing the substrate conversion curves without making the K_i >> [E] assumption.[10,36,37] The kinetic model from Schwartz *et al*. was slightly adapted to incorporate the spontaneous enzyme inactivation observed for blank measurements, where substrate depletion cannot explain the decrease in substrate conversion rate. As the substrate concentration was well below the predicted K_M, the one-step substrate conversion proposed by Schwartz *et al*. was maintained. Initial values for the required rate constants were derived from several preliminary experiments, and were mostly left to be optimized by the algorithm (Figure S4.1).

The assay was validated using irreversible DAGL inhibitors (KT109 and DH376) and a reversible inhibitor (LEI105) (Figure 4.1C). All three inhibitors were previously found to be highly active with (sub)nanomolar potency (pIC_{50} 8.6 to 9).[20,22,38] Using seven inhibitor concentrations around their reported IC_{50}-values, a set of substrate conversion curves was generated. These curves were fitted with DynaFit (Figure S4.1). The resulting fits and values for K_i and k_{inact} are shown in Figure 4.2. As was expected, the model does not find a fit for the k_{inact} value for the covalent but reversible inhibitor LEI105. The found K_i-values (all between 0.2 and 0.4 nM) were generally in line with the high potency described in literature, although LEI105 was somewhat more active than previously reported.[22] The inactivation rates for KT-109 and DH376 were similar (k_{inact} = ± 0.07 min^{-1}).

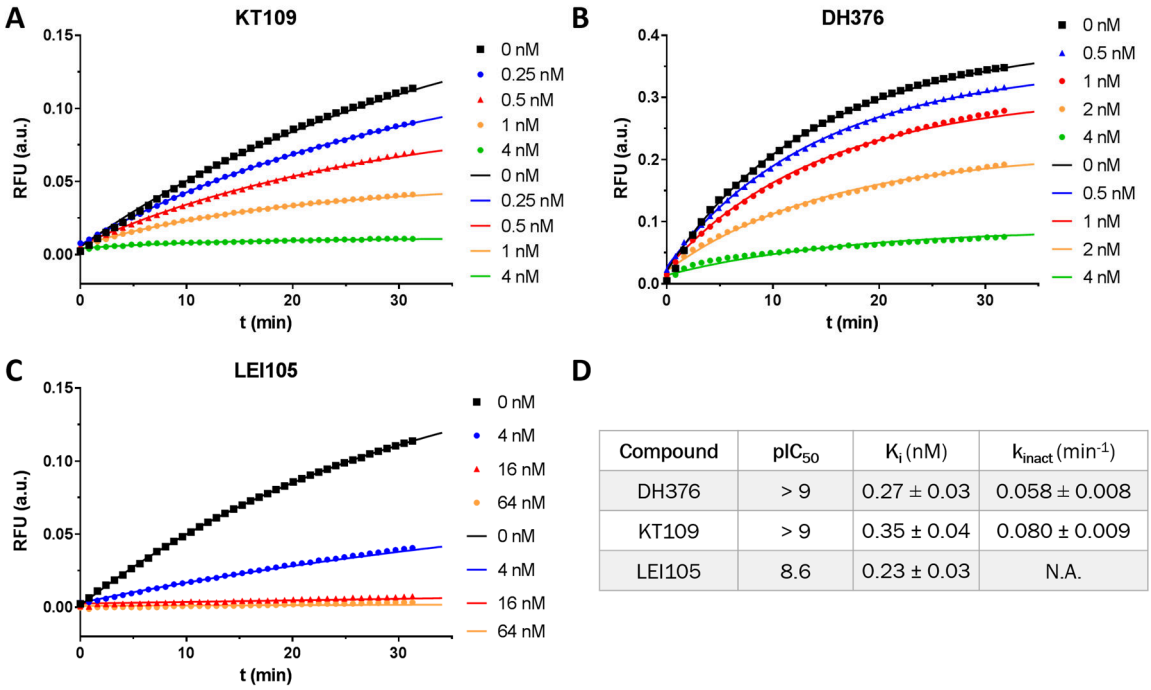

Compound	pIC_{50}	K_i (nM)	k_{inact} (min^{-1})
DH376	> 9	0.27 ± 0.03	0.058 ± 0.008
KT109	> 9	0.35 ± 0.04	0.080 ± 0.009
LEI105	8.6	0.23 ± 0.03	N.A.

Figure 4.2 | Kinetics of binding of KT109 (A), DH376 (B) and LEI105 (C), data fits are summarized in (D). For clarity not all substrate conversion curves used for the curve fitting are shown. Markers denote measured absorbance, lines denote fitted model.

Next, we tested inhibitors **1**-**5** to determine the influence of the leaving group on their potency in the standard surrogate substrate assay. A large range in IC_{50}-values was observed (Figure 4.3A, Table 4.1). Both regioisomers **1** and **2** were low nanomolar inhibitors, whereas the 1,2,4-triazole (**3**) had a reduced potency (IC_{50} = 3.4 μM) and the imidazole (**5**) was inactive (IC_{50} > 10 μM). Pyrazole (**4**) had an intermediate potency with IC_{50} of 0.21 μM. The IC_{50}-values were used to guide the selection of inhibitor concentrations for the kinetic assay (Figure 4.3B, Table 4.1). For all but the imidazole compound **5** we were able to determine the kinetic parameters. Intriguingly, the inactivation rates for **1** and **2** (k_{inact} = 0.22 and 0.32 min^{-1}, respectively), were 2-3 times higher than for KT109 and DH376, but they had a lower binding affinity (Ki = 10 and 339 nM, respectively). Unexpectedly, the inactivation rates for **3** and **4** were comparable to DH376 and KT109, whereas there is 10,000-fold difference in pK_a between these heterocycles (Table 4.1). Yet, the binding affinity of **3** and **4** was substantially reduced (Ki > 10 μM), thereby explaining their higher IC_{50}-values.

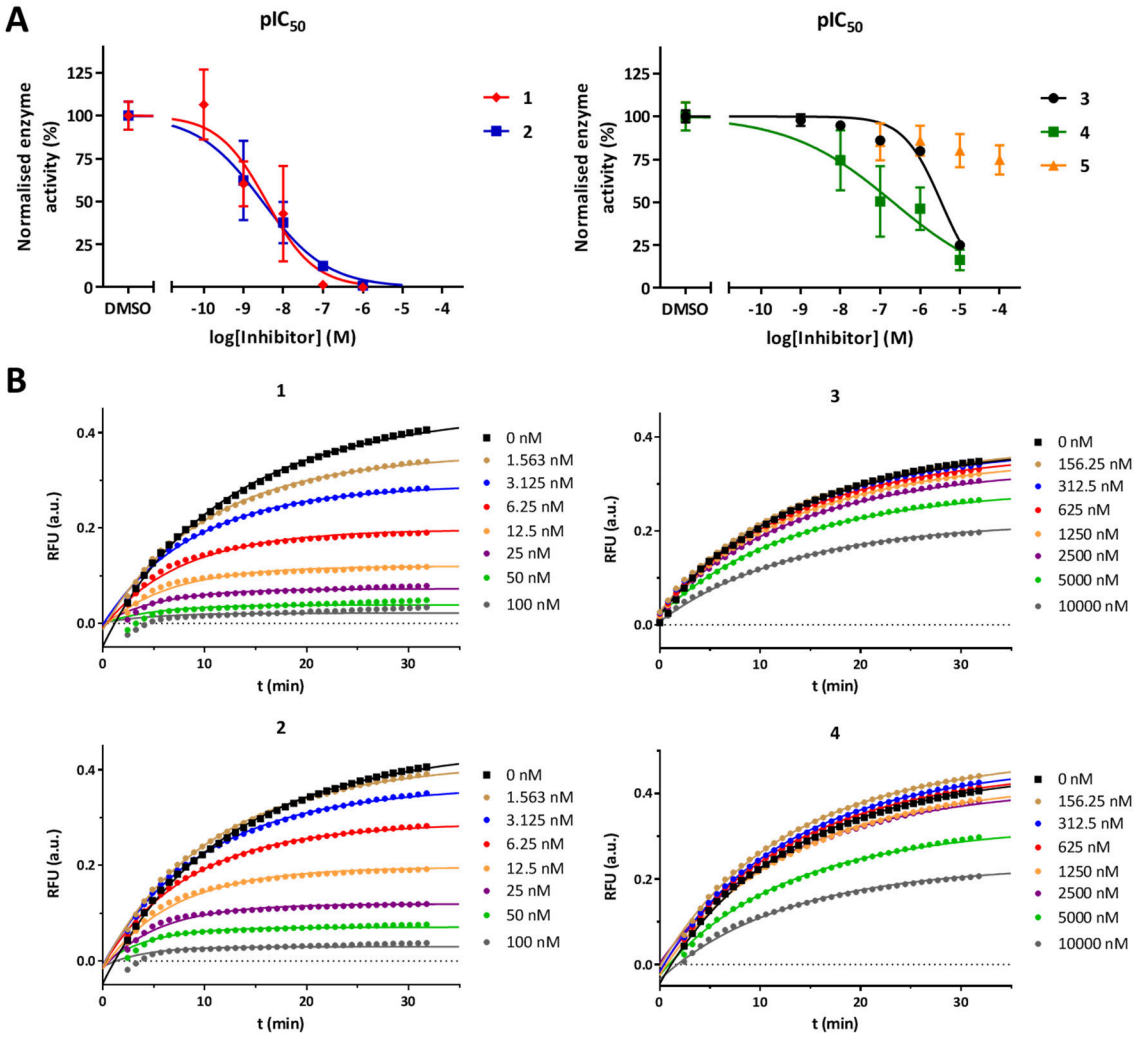

Figure 4.3 | pIC_{50} determination of compounds **1**-**5** (A) and kinetic fits (B). All data points are measured as N = 4, positive controls (DMSO) as N = 8. Markers denote mean values, error bars denote the SEM, lines are fitted data models.

Table 4.1 | Potency and kinetic parameters of the focused set of DH376 derivatives **1-5**.

Compound	pIC_{50}	K_i (nM)	k_{inact} (min^{-1})	pK_a
1	8.52 ± 0.27	10.4 ± 2.0	0.22 ± 0.03	9.3[31]
2	8.42 ± 0.28	339 ± 55	0.32 ± 0.04	9.3[31]
3	5.47 ± 0.07	13770 ± 910	0.075 ± 0.005	10.0[29]
4	6.68 ± 0.41	10800 ± 910	0.080 ± 0.005	14.2[30]
5	< 4.5	N.D.	N.D.	14.4[30]

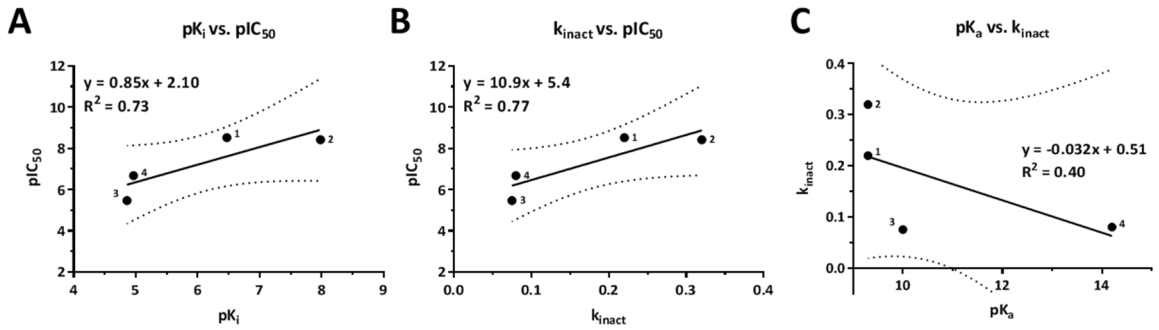

Figure 4.4 | pIC_{50} correlates with both pK_i (A) and k_{inact} (B) but pK_a (C) does not correlate with reactivity for the inhibitors **1-4**. Dashed lines denote 90% confidence interval.

Discussion

We developed a surrogate substrate based assay to determine the kinetic parameters of binding and reactivity of triazole urea inhibitors of the serine hydrolase DAGL-α. Having the ability to discern the kinetics of binding should enable the optimization of the affinity of the inhibitors for the enzyme, the K_i, while controlling the reactivity k_{inact}, to minimize the off-target reactivity. The assay was validated using three well-characterized published DAGL inhibitors. Five DH376 derivatives were synthesized to study the role of the leaving group in the affinity and reactivity with DAGL-α. The IC_{50}-values correlated with the K_i and k_{inact} with an R^2 of 0.73 and 0.77, respectively (Figure 4.4A, B). The main reason for the large differences observed in IC_{50}-values for the five inhibitors was the strong reduction in binding affinity for the pyrazole and 1,2,4-triazole compounds compared to the 1,2,3-triazole inhibitors. Unexpectedly, it was shown that the 1,2,4-triazole **3** and pyrazole **4** inhibitors were as reactive as DH376 and KT109, which is in stark contrast to the five orders of magnitude difference in pK_a. This showed that the leaving group acidity does not correlate with the rate of inactivation k_{inact} (Figure 4.4C).

The triazole heterocycles of DH376 and KT109 could be involved in hydrogen bonds with active site amino acids, as has been previously shown for α-positioned heterocycles for related serine hydrolases like FAAH and others.[39,40] From our kinetic investigation we indeed conclude that the position of the nitrogen atoms in the ring is of great importance for the formation and strength of these bonds. Despite the lack of knowledge of the structure of DAGL-α, we could speculate that a major hydrogen bonding interaction has to occur from the direction in which His650 is drawn in Figure 4.5 (directionality relative to the

heterocycle). His650 is part of the catalytic triad and has been postulated to bind in this manner before, based on the covalent docking of α-ketoheterocycles in a homology model of DAGL-α.[41] The 1,2,3-triazoles would both be capable of forming this bond. Compounds **3**-**5** could not form this interaction, which would explain the strong drop in binding affinity. A second weaker hydrogen bonding interaction on the other side of the urea functionality could explain the further differences observed. A candidate hydrogen bond donor would be His471 (drawn in Figure 4.5).[41] Compound **1** would be optimally positioned to bind both, leading to the low K_i observed. The *N*1-isomer could only bind His650, leading to a slight drop in potency. Compounds **3** and **4** could both bind only through the weaker second interaction, leading to a poor overall binding. Imidazole **5** would be unable to pick up either bond. The proposed hydrogen bonding interactions are unable to directly explain the slight difference in binding between **3** and **4**, though the specific electronic properties of the azoles (i.e. the efficiency of the hydrogen bond formation) could be a cause.

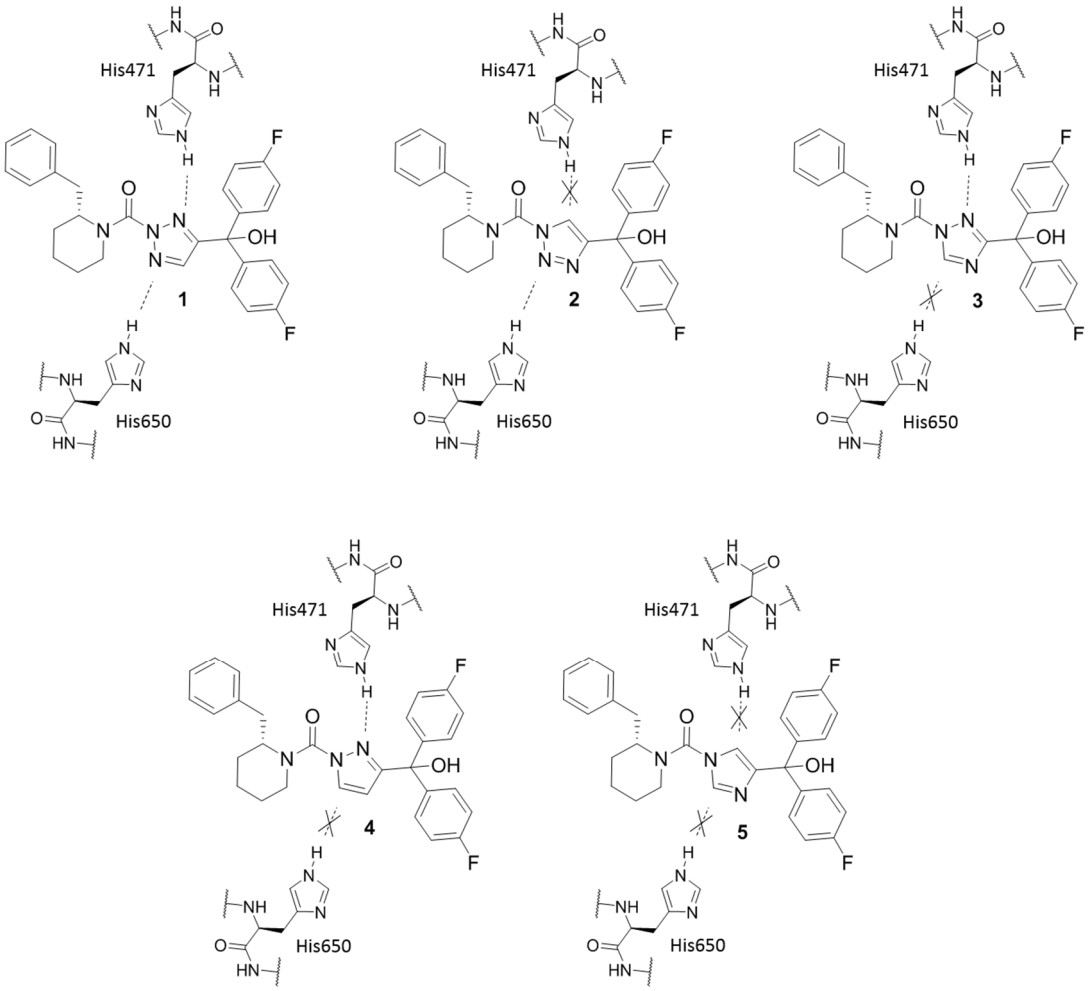

Figure 4.5 | Illustration of the hypotheses using potential hydrogen bonding to explain the difference in K_i. His650 is hypothesized to form the major hydrogen bond; His471 might form a secondary hydrogen bonding interaction.

The assay presented here, in combination with the data analysis through numerical fitting, could be translated to work on a multitude of serine hydrolases. As long as a sensitive and robust (surrogate) substrate assay is available that can be interrogated in a time-dependent manner it should in principle be possible to derive structure kinetics relationships. These relationships provide important insights into the mode of action and can aid in the optimization of covalent serine hydrolase inhibitors in an affinity directed manner. For the DAG lipase inhibitors, this may lead to more selective inhibitors more suitable for further *in vivo* target validation studies.

Conclusion

To conclude, we have developed a kinetic assay to study the influence of the heterocyclic core of triazole ureas as covalent, mechanism-based inhibitors of diacylglycerol lipase-α. We found that the pK_a of the leaving group did not correlate with the reactivity of the inhibitors, but that the position of the nitrogen atom in the heterocycle is of importance in its binding affinity. Detailed knowledge of structure kinetic relationships is expected to guide the optimization of more selective and well-balanced irreversible inhibitors of serine hydrolases.

Acknowledgements

Jacob van Hengst is kindly acknowledged for his essential contribution to the synthetic work described in this Chapter.

Methods

Chemical biology methods

Cell culture and membrane preparation

HEK293T cells were grown in DMEM with stable glutamine and phenolred (PAA) with 10% New Born Calf serum, penicillin and streptomycin. Cells were passaged every 2-3 days by resuspending in medium and seeding them to appropriate confluence. Membranes were prepared from transiently transfected HEK293T cells. One day prior to transfection 10^7 cells were seeded in a 15 cm petri dish. Cells were transfected by the addition of a 3:1 mixture of polyethyleneimine (60 µg) and plasmid DNA (20 µg) in 2 mL serum free medium. The medium was refreshed after 24 hours, and after 72 h the cells were harvested by suspending them in 20 mL medium. The suspension was centrifuged for 10 min at 1000 *g*, and the supernatant was removed. The cell pellet was stored at -80 °C until use.

Cell pellets were thawed on ice and suspended in lysis buffer (20 mM Hepes, 2 mM DTT, 0.25 M sucrose, 1 mM $MgCl_2$, 25 U/mL benzonase). The suspension was homogenized by polytrone (3x 7 sec) and incubated for 30 min on ice. The suspension was subjected to ultracentrifugation (93,000 *g*, 30 min, 4 °C, Beckman Coulter, Type Ti70 rotor) to yield the cytosolic fraction in the supernatant and the membrane fraction as a pellet. The pellet was resuspended in storage buffer (20 mM Hepes, 2 mM DTT). The protein concentration was determined with Quick Start Bradford assay (Biorad). The protein fractions were diluted to a total protein concentration of 1 mg/mL and stored in small aliquots at -80 °C until use.

Surrogate substrate assay

The biochemical mDAGL-α activity assay is based on the method previously described.[32] 100 µL reactions were performed in flat bottom Greiner 96-wells plates in a 50 mM pH 7.2 Hepes buffer. Membrane protein fractions from HEK293T cells transiently transfected with mDAGL-α (0.05 µg/µL final concentration) were used as mDAGL-α source. Inhibitors were introduced in 2.5 µL DMSO. The mixtures were incubated for 20 minutes before 5.0 µL 6 mM PNP-butyrate (final concentration 0.3 mM) in 50% DMSO was added (final DMSO concentration 5.0%). Reactions were allowed to progress for 30 minutes at 20 °C before OD (420 nm) was measured using a TECAN GENios plate reader. All experiments were performed at N=2, n=2 for experimental measurements and N=2, n=4 for controls.

Data analysis: Z'-factor of each plate was determined for the validation of each experiment, using the following formula $Z'=1-3(\sigma_{pc}+\sigma_{nc})/(\mu_{pc}-\mu_{nc})$. The OD from the positive control (pc: DAGL DMSO), and the negative control (nc: 10 µM THL) was used. Plates were accepted for further analysis when Z'>0.6. Measurements were corrected for the average absorption of the negative control (10 µM THL). The average, standard deviation (SD) and standard error of mean (SEM) were calculated and normalized to the corrected positive control. Data was exported to Graphpad Prism 7.0 for the calculation of the pIC_{50} using a non-linear dose-response analysis.

DynaFit setup

DynaFit version 4 was used with an academic license. For batch processing the command line interface was used. The raw data were pre-processed using Microsoft Excel 2016 and exported to tab delimited text files for use with DynaFit. Scripts were generated manually or using a purpose-made python script. An example DynaFit script is shown in Figure S4.1.

The contents of the header [task] follow directly from the DynaFit manual and simply state that the program should fit progress curves using the data supplied.

The section [mechanism] was built based on standard enzyme kinetics. The simplified hit and run (`E + S ---> E + P`) was used for the substrate conversion as the K_M of the surrogate substrate is too high to be determined reliably experimentally.[10,32] The additional enzyme degradation step (`E ---> E*`) was included as the progress rate curves for the DMSO blanks decreased more than could be explained by the reduction in substrate concentration (which is accounted for in the set of differential equations fitted).

The rate constants defined in [constants] were set empirically but are all left to be optimized. The exception is k_{on}, which is fixed to 100,000 $\mu M^{-1} \cdot min^{-1}$, but the variable itself is dependent on k_{off} (and vice versa), so only the ratio of the two (K_i) is physically meaningful in this experimental setup.

As the enzyme is obtained by overexpression in HEK293T cells the exact concentration is unknown. Data from the previously published PNPB-based assay used for pIC_{50} determination indicate that the assay limit lies around 9, which puts the enzyme concentration at ± 1 nM. It is left to be optimised by DynaFit.

The value for P given in the [responses] section is essentially the absorption coefficient of the converted surrogate substrate in $AU \cdot \mu M^{-1}$, which was determined experimentally (Figure S4.2).

Chemistry

General remarks

All reactions were performed using oven- or flame-dried glassware and dry (molecular sieves) solvents. Reagents were purchased from Alfa Aesar, Sigma-Aldrich, Acros, and Merck and used without further purification unless noted otherwise. All moisture sensitive reactions were performed under an argon or nitrogen atmosphere.

^{1}H and ^{13}C NMR spectra were recorded on a Bruker DPX-300 (300 MHz), AV-400 (400 MHz) or DRX-500 (500 MHz). Used software for interpretation of NMR-data was Bruker TopSpin 1.3 and MestreNova 11.0. Chemical shift values are reported in ppm with tetramethylsilane or solvent resonance as the internal standard ($CDCl_3$: δ 7.26 for ^{1}H, δ 77.16 for ^{13}C; ACN-*d*3: δ 1.94 for ^{1}H, δ 1.32 for ^{13}C; MeOD: δ 3.31 for ^{1}H, δ 49.00 for ^{13}C).[42] Data are reported as follows: chemical shifts (δ), multiplicity (s = singlet, d = doublet, dd = double doublet, td = triple doublet, t = triplet, q = quartet, bs = broad singlet, m = multiplet), coupling constants *J* (Hz), and integration.

Liquid chromatography was performed on a Finnigan Surveyor LC/MS system, equipped with a C18 column. Flash chromatography was performed using SiliCycle silica gel type SiliaFlash P60 (230–400 mesh). TLC analysis was performed on Merck silica gel 60/Kieselguhr F254, 0.25 mm. Compounds were visualized using $KMnO_4$ stain (K_2CO_3 (40 g), $KMnO_4$ (6 g), and water (600 mL)) or CAM stain ($Ce(NH_4)_4(SO_4)_4{\cdot}2H_2O$ (ceric ammonium sulfate: 10 g); ammonium molybdate (25 g); conc. H_2SO_4 (100 mL); H_2O (900 mL)). Preparative HPLC (Waters, 515 HPLC pump M; Waters, 515 HPLC pump L; Waters, 2767 sample manager; Waters SFO System Fluidics Organizer; Waters Acquity Ultra Performance LC, SQ Detector; Waters Binary Gradient Module) was performed on a Waters XBridgeTM column (5 µM C18, 150 x 19 mm). Diode detection was done between 210 and 600 nm. Gradient: ACN in (H_2O + 0.2% TFA). Chiral HPLC analysis was performed after benzoylation of the free amine on a Daicel Chiralpak AD column (250 x 4.5 mm, 10 µm particle size) using 10 % isopropyl alcohol in hexane as eluent (1.0 mL/min, UV-detection at 254 nm) Rt= 15.1 min (*R*-enantiomer 12.8 min). High resolution mass spectra (HRMS) were recorded by direct injection on a q-TOF mass spectrometer (Synapt G2-Si) equipped with an electrospray ion source in positive mode with Leu-enkephalin (m/z = 556.2771) as an internal lock mass. The instrument was calibrated prior to measurement using the MS/MS spectrum of Glu-1-fibrinopeptide B.

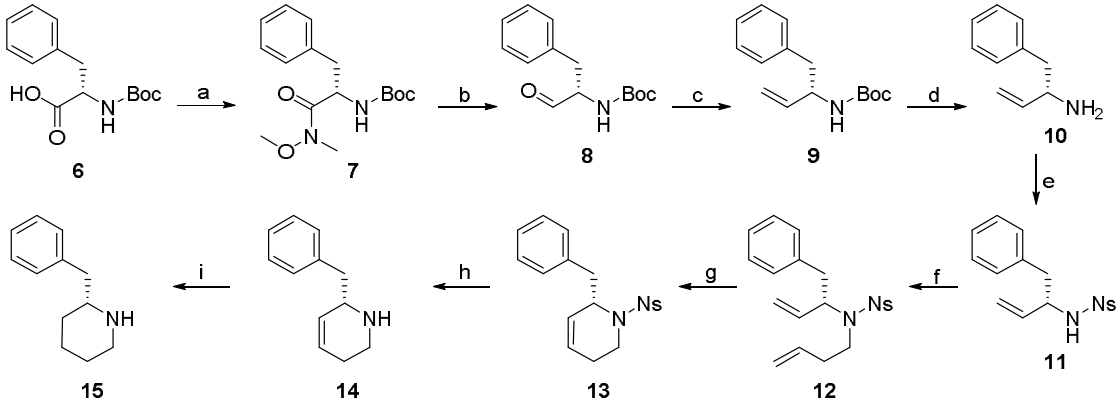

Scheme S4.1 | Synthesis of (*R*)-2-benzylpiperidine. Reagents and conditions: a) *N,O*-di-Me-hydroxylamine·HCl, EDCI·HCl, DCM, 0 °C → RT, 92%; b) $LiAlH_4$, THF, -20 °C, 96%; c) $MeP(Ph)_3.Br$, KHMDS, THF, -78 °C → RT, 56%; d) HCl, $MeOH/H_2O$, quant.; e) NsCl, NEt_3, DMAP, DCM 85%; f) 4-bromobut-1-ene, K_2CO_3, DMF; 70 °C, 80%; g) Grubbs' 1st gen., DCM, 40 °C, 62%; h) PhSH, NaOH, ACN/H_2O, 50 °C, 99%; i) $RuCl_3(H_2O)_3$, $NaBH_4$, DCE/MeOH, 87%.

tert-Butyl (*S*)-(1-(methoxy(methyl)amino)-1-oxo-3-phenylpropan-2-yl)carbamic acid (7)

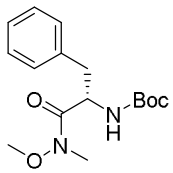

N-Boc-L-phenylalanine **6** (24.16 g, 91 mmol), *N,O*-dimethylhydroxylamine hydrochloride (9.95 g, 102 mmol) and 4-methylmorpholine (11.25 mL, 102 mmol) were dissolved in dichloromethane and cooled to 0 °C. EDCI·HCl (18.75 g, 98 mmol) was added in three portions with a 15 min interval. After consumption of the starting material, the reaction mixture was washed with sat. aq. NH_4Cl, sat. aq. $NaHCO_3$ and brine. The organic phase was dried ($MgSO_4$), filtered and concentrated under reduced pressure to obtain the pure title compound as a honey like oil (25.9 g, 84 mmol, 92%).^{1}H NMR (400 MHz, $CDCl_3$) δ 7.36 – 7.06 (m, 7H), 5.04 – 4.85 (m, 1H), 3.65 (s, 3H), 3.17 (s, 3H), 3.09 – 2.96 (m, 1H), 2.94 – 2.80 (m, 1H), 1.37 (s, 11H). ^{13}C NMR (101 MHz, $CDCl_3$) δ 155.27, 136.70, 129.56, 128.45, 126.86, 79.67, 61.65, 51.62, 43.93, 38.97, 28.42.

tert-Butyl (*S*)-(1-oxo-3-phenylpropan-2-yl)carbamate (**8**)

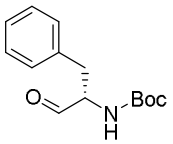

7 (25.9 g, 84 mmol) was dissolved in THF and cooled to -15 °C. Subsequently a 1 M solution of $LiAlH_4$ in THF (42 mL, 42 mmol) was added slowly. Upon completion, the reaction was quenched with 25% aq. $KHSO_4$, allowed to warm up to RT and stirred vigorously. Ethyl acetate was added, and the organic phase was separated, washed with sat. aq. $NaHCO_3$ and brine, dried ($MgSO_4$), filtered and concentrated under reduced pressure to give the title compound as a white solid. (20.2 g, 81 mmol, 96%). ^{1}H NMR (400 MHz, $CDCl_3$) δ 9.63 (s, 1H), 7.43 – 7.04 (m, 5H), 5.18 – 4.99 (m, 1H), 4.43 (q, *J* = 6.8 Hz, 1H), 3.12 (d, *J* = 6.7 Hz, 2H), 1.41 (s, 9H). ^{13}C NMR (101 MHz, $CDCl_3$) δ 199.56, 135.90, 129.46, 128.88, 127.19, 80.33, 60.91, 35.58, 28.39.

tert-Butyl (*S*)-(1-phenylbut-3-en-2-yl)carbamate (**9**)

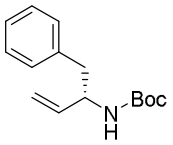

To a solution of potassium bis(trimethylsilyl)amide (27 g, 135 mmol) in dry THF was added methyltriphenylphosphonium bromide (54.8 g, 153 mmol). The resulting mixture was stirred for 3 hr and subsequently cooled to -78 °C, after which a solution of **8** (22.5 g, 90 mmol) in THF was added. The reaction was allowed to warm up to RT overnight and quenched with sat. aq. NH_4Cl. EtOAc was added and the organic phase was separated, washed with sat. aq. $NaHCO_3$ and brine, dried ($MgSO_4$), filtered and concentrated under reduced pressure. The residue was purified with silica chromatography (8% ethyl acetate in petroleum ether) to give the desired product as a white, waxy solid (12.6 g, 50.9 mmol, 56%). ^{1}H NMR (400 MHz, $CDCl_3$) δ 7.34 – 7.13 (m, 5H), 5.88 – 5.71 (m, 1H), 5.16 – 5.03 (m, 2H), 4.45 (d, *J* = 27.0 Hz, 2H), 2.83 (d, *J* = 6.5 Hz, 2H), 1.40 (s, 9H). ^{13}C NMR (101 MHz, $CDCl_3$) δ 155.33, 138.18, 137.53, 129.68, 128.44, 126.59, 114.84, 79.53, 53.58, 41.60, 28.47.

(*S*)-1-Phenylbut-3-en-2-amine (**10**)

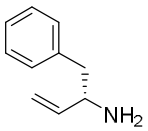

9 (9.7 g, 39.2 mmol) was dissolved in absolute methanol and 4 M aq. HCl was added. After TLC showed full consumption of the starting material, the mixture was concentrated under reduced pressure and diluted with water. The solution was washed with diethyl ether and aq. NaOH was used to make the aqueous layer basic (pH > 12). The aqueous phase was extracted 3x with chloroform. The organic layers were combined, dried ($MgSO_4$), filtered and concentrated under reduced pressure to give the title compound in quantitative yield. Epimerised product that was formed during Wittig olefination was removed by recrystallization form toluene/n-propyl alcohol with *N*-acetyl-L-leucine according to literature procedure,[43] yielding the amine as a yellow oil with an enantiomeric ratio of 97:3 as determined by chiral HPLC (*vide infra*). ^{1}H NMR (400 MHz, $CDCl_3$) δ 7.36 – 7.12 (m, 5H), 5.89 (ddd, *J* = 16.8, 10.3, 6.2 Hz, 1H), 5.14 (dt, *J* = 17.2, 1.5 Hz, 1H), 5.04 (dt, *J* = 10.3, 1.4 Hz, 1H), 3.64 – 3.52 (m, 1H), 2.83 (dd, *J* = 13.3, 5.4 Hz, 1H), 2.62 (dd, *J* = 13.3, 8.3 Hz, 1H), 1.31 (s, 3H). ^{13}C NMR (101 MHz, $CDCl_3$) δ 142.49, 138.86, 129.51, 128.50, 126.45, 113.77, 55.57, 44.43.

Before recrystallization

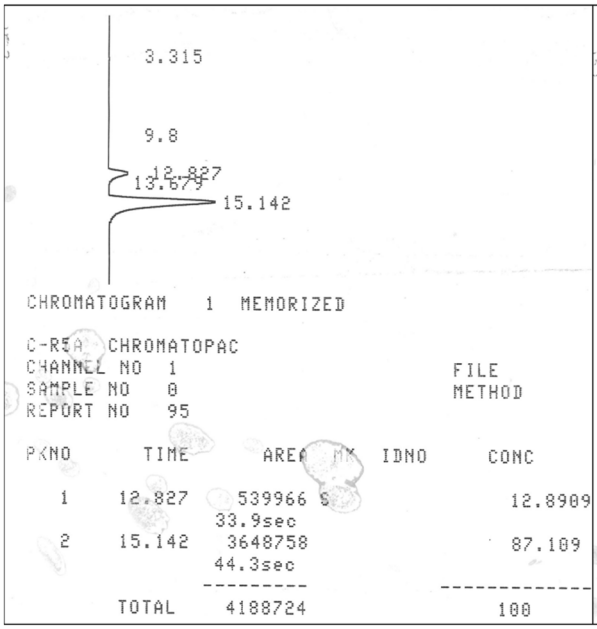

After recrystallization

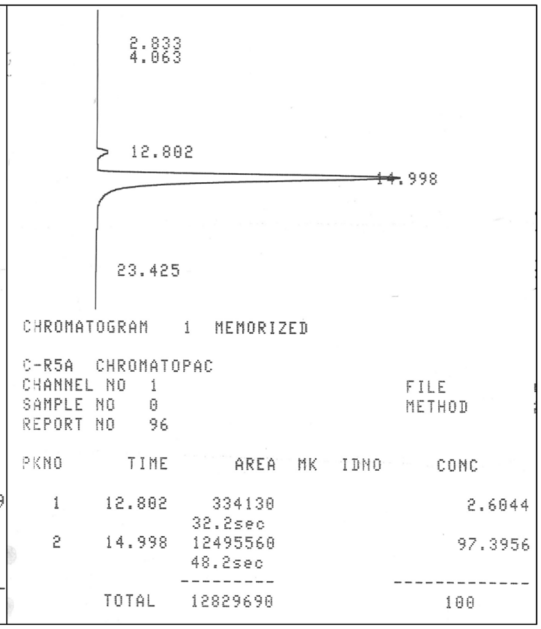

(*S*)-2-Nitro-*N*-(1-phenylbut-3-en-2-yl)benzenesulfonamide (**11**)

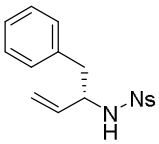

10 (3.5 g, 23.8 mmol), triethylamine (4.88 mL, 35.7 mmol), *N,N*-dimethylaminopyridine (1.45 g, 11.9 mmol) and 2-nitrobenzenesulphonyl chloride (6.85 g, 30.9 mmol) were dissolved in dry DCM and stirred overnight, after which the reaction mixture was concentrated under reduced pressure. Flash column chromatography (20% ethyl acetate in petroleum ether) yielded the desired product with trace impurities as an orange oil (6.7 g, 20 mmol, 85%). ^{1}H NMR (400 MHz, $CDCl_3$) δ 8.01 – 7.90 (m, 1H), 7.83 – 7.71 (m, 1H), 7.69 – 7.58 (m, 2H), 7.18 – 7.01 (m, 5H), 5.81 – 5.64 (m, 1H), 5.40 (d, *J* = 7.9 Hz, 1H), 5.13 (dt, *J* = 17.1, 1.2 Hz, 1H), 5.03 (dt, *J* = 10.3, 1.1 Hz, 1H), 4.32 – 4.17 (m, 1H), 2.92 (dd, *J* = 13.8, 6.1 Hz, 1H), 2.79 (dd, *J* = 13.8, 7.8 Hz, 1H). ^{13}C NMR (101 MHz, $CDCl_3$) δ 137.21, 136.22, 134.84, 133.22, 132.92, 130.79, 129.46, 128.54, 127.03, 125.53, 116.57, 58.68, 42.16.

(*S*)-*N*-(But-3-en-1-yl)-2-nitro-*N*-(1-phenylbut-3-en-2-yl)benzenesulfonamide (**12**)

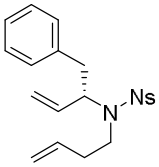

11 (6.7g, 20.2 mmol) was dissolved in DMF and K_2CO_3 (11.1 g, 81 mmol) and 4-bromo-1-butene (2.46 mL, 24.2 mmol) were added. The mixture was heated to 70 °C and stirred vigorously. After 24 hr, an extra portion of 4-bromo-1-butene (2.46 mL, 24.2 mmol) was added and the resulting mixture was stirred for 72 h. The reaction was allowed to cool down to RT, diluted with brine and extracted 3x with EtOAc. Combination, drying ($MgSO_4$), filtration and concentration of the organic phases yielded the desired product as a brown oil (6.24 g, 16.2 mmol, 80%). ^{1}H NMR (400 MHz, $CDCl_3$) δ 7.92 – 7.84 (m, 1H), 7.69 – 7.52 (m, 3H), 7.25 – 7.12 (m, 5H), 5.89 – 5.64 (m, 2H), 5.17 – 5.02 (m, 4H), 4.72 – 4.62 (m, 1H), 3.50 – 3.31 (m, 2H), 3.08 (dd, *J* = 13.5, 5.9 Hz, 1H), 2.95 (dd, *J* = 13.5, 9.2 Hz, 1H), 2.50 – 2.31 (m, 2H). ^{13}C NMR (101 MHz, $CDCl_3$) δ 137.45, 135.28, 134.61, 134.09, 133.45, 131.70, 130.88, 129.39, 128.55, 126.75, 124.29, 118.98, 117.34, 61.66, 44.69, 39.60, 35.63.

(*S*)-6-Benzyl-1-((2-nitrophenyl)sulfonyl)-1,2,3,6-tetrahydropyridine (**13**)

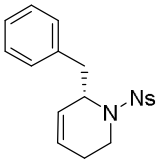

A solution of **12** (6.24 g, 16.2 mmol) in DCM was purged with argon and 1st generation Grubbs catalyst (400 mg, 3 mol%) was added. The mixture was heated to 40 °C and stirred overnight. Volatiles were removed under reduced pressure and flash column chromatography (40% diethyl ether in petroleum ether) yielded the desired product as brown powder (3.57 g, 9.96 mmol, 62%). ^{1}H NMR (400 MHz, $CDCl_3$) δ 7.85 (d, *J* = 7.7 Hz, 1H), 7.69 – 7.48 (m, 3H), 7.25 – 7.09 (m, 5H), 5.87 – 5.74 (m, 1H), 5.62 (d, *J* = 10.6 Hz, 1H), 4.56 (s, 1H), 3.93 (dd, *J* = 14.4, 6.2 Hz, 1H), 3.15 (ddd, *J* = 15.2, 11.7, 4.1 Hz, 1H), 3.00 (dd, *J* = 13.1, 6.0 Hz, 1H), 2.89 (dd, *J* = 13.1, 8.3 Hz, 1H), 2.21 – 2.04 (m, 1H), 1.93 (dt, *J* = 18.1, 5.0 Hz, 1H). ^{13}C NMR (101 MHz, $CDCl_3$) δ 137.28, 134.48, 133.30, 131.84, 130.44, 129.69, 128.50, 127.27, 126.79, 125.61, 124.27, 55.78, 41.71, 39.11, 24.33.

(*S*)-6-Benzyl-1,2,3,6-tetrahydropyridine (**14**)

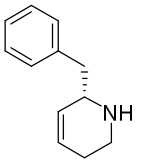

To a solution of thiophenol (2.56 mL, 24.9 mmol) in acetonitrile cooled with ice was added a 2 M aq. solution of NaOH (12.45 mL, 24.9 mmol). After stirring for 10 minutes, the ice bath was removed and a solution of **13** (3.57 g, 9.96 mmol) in acetonitrile was added slowly. The resulting mixture was heated to 50 °C. When TLC showed full conversion of the starting material, the reaction was cooled to RT and diluted with aq. HCl so that the pH was below 2. The aqueous layer was washed with Et_2O and diluted with aq. NaOH until the pH was above 12. It was then extracted 3x with ethyl acetate. The organic layers were combined, dried ($MgSO_4$), filtered and concentrated to afford the desired product as yellow oil (1.71 g, 9.86 mmol, 99%). ^{1}H NMR (400 MHz, $CDCl_3$) δ 7.37 – 7.15 (m, 5H), 5.84 – 5.75 (m, 1H), 5.64 (dq, *J* = 10.1, 2.0 Hz, 1H), 3.61 – 3.51 (m, 1H), 3.17 – 2.99 (m, 1H), 2.85 – 2.75 (m, 2H), 2.70 (dd, *J* = 13.2, 8.8 Hz, 1H), 2.26 – 2.12 (m, 1H), 2.02 – 1.91 (m, 1H). ^{13}C NMR (101 MHz, $CDCl_3$) δ 138.97, 130.25, 129.39, 128.57, 126.43, 126.22, 55.47, 42.56, 42.12, 25.86.

(*R*)-2-Benzylpiperidine (**15**)

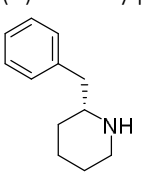

In a three-neck flask containing two stoppers and one septum with empty balloons, **14** (1.70 g, 9.81 mmol) was dissolved in dichloroethane/methanol 10:3. This solution was purged with argon and cooled to 0 °C, after which $RuCl_3(H_2O)_3$ (257 mg, 0.98 mmol) was added. $NaBH_4$ (1.86 g, 49 mmol) was added quickly while capturing the formed H_2 gas in the empty balloons, thus keeping the reaction under hydrogen atmosphere. The reaction was allowed to warm up to RT and stirred overnight. Aqueous HCl was then added, so that the water layer had a pH of

below 2. The aqueous layer was washed with Et_2O and diluted with aq. NaOH until the pH was above 12. The water layer was extracted thrice with ethyl acetate. The organic layers were combined, dried ($MgSO_4$), filtered and concentrated to yield the title compound as a yellow waxy solid (1.5 g, 8.6 mmol, 87%). ^{1}H NMR (400 MHz, $CDCl_3$) δ 7.38 – 7.03 (m, 5H), 3.08 – 2.89 (m, 1H), 2.77 – 2.64 (m, 2H), 2.64 – 2.46 (m, 2H), 1.84 – 1.73 (m, 1H), 1.73 – 1.63 (m, 1H), 1.63 – 1.52 (m, 1H), 1.52 – 1.38 (m, 1H), 1.37 – 1.15 (m, 3H). ^{13}C NMR (101 MHz, $CDCl_3$) δ 139.12, 129.23, 128.39, 126.20, 58.26, 47.08, 43.81, 32.77, 26.08, 24.80.

Methyl 1*H*-1,2,3-triazole-4-carboxylate (**17**)

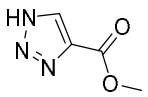

This protocol was based on literature procedure.[44] A mixture of azidotrimethylsilane (2.6 mL, 20 mmol) and methyl propiolate **16** (1.8 mL, 20 mmol) was heated for 4 h at 90 °C, concentrated and coevaporated with MeOH to yield the title compound as a white solid (1.74 g, 14 mmol, 68%). ^{1}H NMR (400 MHz, MeOD) δ 8.35 (s, 1H), 3.92 (s, 3H). ^{13}C NMR (101 MHz, MeOD) δ 162.61, 139.63, 131.92, 52.53.

Bis(4-fluorophenyl)(1*H*-1,2,3-triazol-4-yl)methanol (**18**)

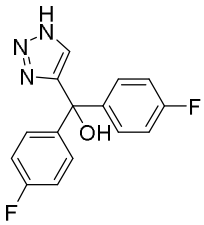

17 (100 mg, 0.787 mmol) was dissolved in THF and cooled to 0 °C. Under vigorous stirring, a 2M solution of 4-fluorophenylmagnesium bromide in Et_2O (1.38 mL, 2.75 mmol) was added dropwise. The reaction mixture was allowed to warm up to RT and stirred overnight. The reaction was quenched with sat. aq. NH_4Cl. The aqueous phase was extracted with DCM (3x). The combined organic layers were dried ($MgSO_4$), filtered and concentrated under reduced pressure. The residue was purified using flash column chromatography (40% to 60% ethyl acetate in pentane) in order to obtain the title compound as a white solid (210 mg, 0.731 mmol, 94%). ^{1}H NMR (400 MHz, MeOD) δ 7.60 (s, 1H), 7.45 – 7.33 (m, 4H), 7.15 – 6.98 (m, 4H).

Methyl 1*H*-1,2,4-triazole-3-carboxylate (**20**)

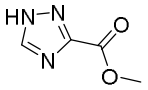

1*H*-1,2,4-triazole-3-carboxylic acid **19** (250 mg, 2.21 mmol) was dissolved in MeOH (50 mL) and cooled to 0 °C. Thionyl chloride (0.48 ml, 6.6 mmol) was slowly added to the solution. The mixture was then heated to reflux for 3 h after which it was cooled to RT and concentrated *in vacuo* to yield the title compound (271 mg, 2.14 mmol, 97%) as a white solid. ^{1}H NMR (400 MHz, MeOD) δ 9.24 (s, 1H), 4.05 (s, 3H).

Bis(4-fluorophenyl)(1*H*-1,2,4-triazol-3-yl)methanol (**21**)

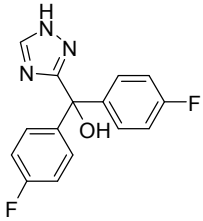

20 (100 mg, 0.787 mmol) was dissolved in THF and cooled to 0 °C. Under vigorous stirring, a 2 M solution of 4-fluorophenylmagnesium bromide in Et_2O (1.37 mL, 2.75 mmol) was added dropwise. The reaction mixture was allowed to warm up to RT and stirred overnight. The reaction was quenched with sat. aq. NH_4Cl. The aqueous phase was extracted with ethyl acetate (3x). The combined organic layers were dried ($MgSO_4$), filtered and concentrated under reduced pressure, yielding the title compound as an off-white solid (201 mg, 0.700 mmol, 89%). ^{1}H NMR (400 MHz, CD_3CN) δ 8.21 (s, 1H), 7.40 (dd, *J* = 8.7, 5.4 Hz, 4H), 7.08 (t, *J* = 8.7 Hz, 4H). ^{13}C NMR (101 MHz, MeOD) δ 163.23, 160.78, 140.15, 133.42, 128.89 (d, *J* = 8.2 Hz), 115.17, 114.42 (d, *J* = 21.7 Hz), 76.63.

1*H*-Pyrazole-3-carboxylic acid (**23**)

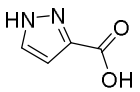

Synthesis based on published procedure.[45] 3-Methyl-1*H*-pyrazole **22** (750 mg, 9.13 mmol) was dissolved in water, $KMnO_4$ (3.18 g, 20.1 mmol) was added and the mixture was refluxed overnight. The reaction was cooled to room temperature, solids were filtered off, and the solvent was removed under reduced pressure. The resulting white powder was used directly without further purification.

Ethyl 1*H*-pyrazole-3-carboxylate (**24**)

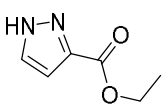

Crude **23** was dissolved in anhydrous ethanol with a catalytic amount of concentrated H_2SO_4 and refluxed overnight. The reaction was allowed to cool to RT, the solvent was partially removed and the residue was neutralized using sat. aq. $NaHCO_3$. The aqueous phase was extracted with ethyl acetate (3x), and the combined organic layers were dried ($MgSO_4$),

filtered and concentrated under reduced pressure, yielding the title compound as a white power (607 mg, 4.33 mmol, 47% over 2 steps). ^{1}H NMR (400 MHz, MeOD) δ 7.73 (d, *J* = 2.3 Hz, 1H), 6.85 (d, *J* = 2.3 Hz, 1H), 4.39 (q, *J* = 7.1 Hz, 2H), 1.40 (t, *J* = 7.1 Hz, 3H). ^{13}C NMR (101 MHz, MeOD) δ 108.84, 105.15, 61.94, 14.58.

Bis(4-fluorophenyl)(1*H*-pyrazol-3-yl)methanol (**25**)

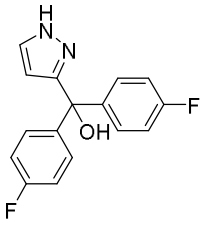

24 (103 mg, 0.735 mmol) was dissolved in THF and cooled to 0 °C. Under vigorous stirring, a 2 M solution of 4-fluorophenylmagnesium bromide in Et_2O (1.29 mL, 2.57 mmol) was added dropwise. The reaction mixture was allowed to warm to RT and stirred overnight. The reaction was quenched with sat. aq. NH_4Cl. The aqueous phase was extracted with DCM (3x). Combined organic layers were dried ($MgSO_4$), filtered and concentrated under reduced pressure. The residue was purified using silica flash chromatography (30% to 60% EtOAc in pentane) yielding the title compound as yellowish solid (175 mg, 0.611 mmol, 83%). ^{1}H NMR (400 MHz, $CDCl_3$) δ 8.08 (s, 1H), 7.24 – 7.10 (m, 5H), 7.03 – 6.85 (m, 4H), 5.83 (d, *J* = 2.2 Hz, 1H). ^{13}C NMR (101 MHz, MeOH) δ 162.18 (d, *J* = 246.8 Hz), 141.90 (d, *J* = 3.1 Hz), 131.77, 129.21 (d, *J* = 8.1 Hz), 114.90 (d, *J* = 21.4 Hz), 110.10, 105.43, 77.61.

Ethyl 1-trityl-1*H*-imidazole-4-carboxylate (**27**)

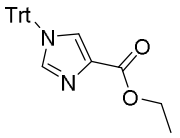

Ethyl 1*H*-imidazole-4-carboxylate **26** (100 mg, 0.714 mmol) was dissolved in DCM at 0 °C, after which trityl chloride (199 mg, 0.713 mmol) and triethylamine (0.117 mL, 0.856 mmol) were added. The reaction mixture was allowed to warm up to RT overnight, after which it was quenched with water. The organic phase was separated, dried ($MgSO_4$), filtered and concentrated under reduced pressure, giving the title compound as a white powder (265 mg, 0.693 mmol, 97%). ^{1}H NMR (400 MHz, $CDCl_3$) δ 7.59 (d, *J* = 1.4 Hz, 1H), 7.45 (d, *J* = 1.4 Hz, 1H), 7.40 – 7.32 (m, 9H), 7.16 – 7.06 (m, 6H), 4.35 (q, *J* = 7.1 Hz, 2H), 1.37 (t, *J* = 7.1 Hz, 3H).

Bis(4-fluorophenyl)(1-trityl-1*H*-imidazol-4-yl)methanol (**28**)

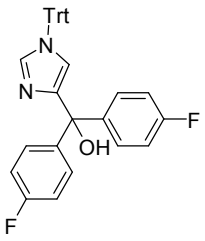

27 (265 mg, 0.693 mmol) was dissolved in THF and cooled to 0 °C. Under vigorous stirring, a 2 M solution of 4-fluorophenylmagnesium bromide in Et_2O (1.38 mL, 2.75 mmol) was added dropwise. The reaction mixture was allowed to warm up to RT and further stirred overnight. The reaction was quenched with sat. aq. NH_4Cl. The aqueous phase was extracted 3x with ethyl acetate. The combined organic layers were dried ($MgSO_4$), filtered and concentrated under reduced pressure. The residue was purified over silica column (50 % EtOAc in pentane) in order to obtain the product as a yellowish powder (315 mg, 0.596 mmol, 86%). ^{1}H NMR (400 MHz, $CDCl_3$) δ 7.85 (s, 1H), 7.47 – 7.27 (m, 10H), 7.23 – 6.83 (m, 13H), 6.20 (s, 1H). ^{13}C NMR (101 MHz, $CDCl_3$) δ 162.18 (d, *J* = 246.9 Hz), 144.16, 140.79, 140.65, 129.62, 129.10 (d, *J* = 8.1 Hz), 128.92, 128.68, 121.17, 115.33, 115.28 – 114.61 (m), 76.24.

Bis(4-fluorophenyl)(1*H*-imidazol-4-yl)methanol (**29**)

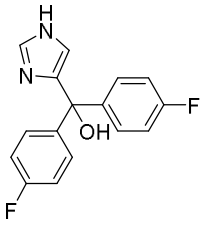

28 (275 mg, 0.520 mmol) was dissolved in 50% TFA/DCM with a few mL of water and stirred overnight. Solvents were removed under reduced pressure and the crude product was dissolved in diethyl ether and extracted with a 1 M aq. HCl solution. The aqueous phase was made basic (pH > 12) with NaOH and extracted with ethyl acetate (3x). Combination, drying ($MgSO_4$), filtered and concentration of the organic phases afforded crude product that was of sufficient purity to use in subsequent reactions as judged by LC/MS (83 mg, 0.29 mmol, 56%).

4-([1,1'-Biphenyl]-4-yl)-1*H*-1,2,3-triazole (**30**)

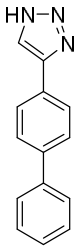

A mixture of formaldehyde (12.5 mL, 168 mmol), acetic acid (1.44 ml, 25.2 mmol) and 1,4-dioxane (125 mL) was stirred for 15 min. Sodium azide (1.64 g, 25.2 mmol) was added, followed by 4-ethynyl-1,1'-biphenyl (3.00 g, 16.8 mmol). After 10 min, sodium ascorbate (0.667 g, 3.37 mmol), and $CuSO_4{\cdot}5H_2O$ (0.210 g, 0.842 mmol) in 1 mL of water were added. The resulting mixture was stirred for 18 h at RT. It was diluted with H_2O (60 mL) and extracted with chloroform (3x 30 mL). The combined organic layers were dried ($MgSO_4$), filtered and concentrated. The residue was suspended in 2 M NaOH (6 mL) and stirred for 20 h at RT. The reaction was acidified with 4 M HCl (aq.) and the white precipitate was filtered off, yielding the desired product as a white solid (2.31 g, 10.4 mmol, 62%). ^{1}H NMR (400 MHz, DMSO) δ 15.18 (s, 1H), 8.40 (s, 1H), 7.99 – 7.93 (m, 2H), 7.81 – 7.75 (m, 2H), 7.75 – 7.69 (m, 2H), 7.53 – 7.45 (m, 2H), 7.42 – 7.34 (m, 1H). ^{13}C NMR (101 MHz, DMSO) δ 156.90, 145.31, 139.56, 128.99, 127.60, 127.17, 126.56, 126.09.

(*R,S)*-2-Benzylpiperidine (**31**)

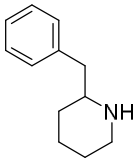

2-Benzylpyridine (5.0 mL, 31 mmol) was dissolved in ethanol (100 mL) and concentrated aqueous HCl (10 mL) was added. Then PtO_2 (112 mg, 0.49 mmol) was added and the mixture was shaken under a hydrogen atmosphere of 2 bar at RT. After overnight shaking, solids were filtered off over celite. The solvent was removed under reduced pressure and the residue was purified using flash column chromatography (10% methanol in DCM) to yield the title compound (4.2 g, 20 mmol, 64%). ^{1}H NMR (300 MHz, $CDCl_3$) δ 8.41 (s, 1H), 7.42 – 7.13 (m, 5H), 3.58 – 3.38 (m, 2H), 3.25 – 3.02 (m, 1H), 3.02 – 2.73 (m, 2H), 2.14 – 1.47 (m, 5H), 1.47 – 1.10 (m, 1H). ^{13}C NMR (75 MHz, $CDCl_3$) δ 136.16, 129.51, 128.76, 127.04, 58.59, 45.11, 40.07, 27.97, 22.61.

General procedure 1: triphosgene coupling of 2-benzylpiperidine and bis(4-fluorophenyl) heterocycle

Triphosgene (0.7 eq.) was dissolved in dry DCM (0.1 M) and to this solution 2-benzylpiperidine (1 eq.) and Na_2CO_3 (1 eq.) were added at 0 °C. The mixture was stirred for 1 hour, warming to RT. The mixture was then filtered and concentrated *in vacuo*. The residue was taken up in dry THF, followed by addition of a bis(4-fluorophenyl)heterocycle (1 eq.), DMAP (0.1 eq.) and DIPEA (1.1 eq.). The reaction mixture was refluxed to completion. The reaction was quenched with saturated NH_4Cl (aq.), after which the water layer was extracted three times with EtOAc. The combined organic layers were washed with brine, dried with $MgSO_4$, filtered and concentrated under reduced pressure.

(*R*)-(2-Benzylpiperidin-1-yl)(4-(bis(4-fluorophenyl)(hydroxy)methyl)-2*H*-1,2,3-triazol-2-yl)methanone (**1**) and (*R*)-(2-benzylpiperidin-1-yl)(4-(bis(4-fluorophenyl)(hydroxy)methyl)-1*H*-1,2,3-triazol-1-yl)methanone (**2**)

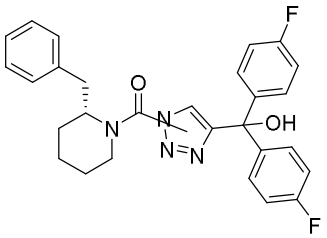

Synthesized according to General Procedure 1 from **18** (123 mg, 0.428 mmol). The *N*1-isomer was isolated as first eluting isomer (1.63 mg, 3.3 µmol, 1.2%). ^{1}H NMR (400 MHz, $CDCl_3$) δ 7.41 – 6.57 (m, 14H), 4.76 (s, 1H), 4.40 – 4.18 (m, 1H), 3.56 (d, J = 66.9 Hz, 1H), 3.41 – 2.81 (m, 2H), 2.65 (s, 1H), 2.08 – 1.39 (m, 6H). HRMS: Calculated for $[C_{28}H_{26}F_2N_4O_2+H]^+$ = 488.2079, found = 488.2090. *N*2-isomer (2.14 mg, 4.4 µmol, 1.5%): ^{1}H NMR (400 MHz, $CDCl_3$) δ 7.48 (s, 1H), 7.40 – 6.70 (m, 13H), 5.04 – 3.66 (m, 2H), 3.47 (s, 1H), 3.26 (t, *J* = 13.3 Hz, 1H), 3.16 – 2.81 (m, 2H), 1.94 – 1.43 (m, 6H). HRMS: Calculated for $[C_{28}H_{26}F_2N_4O_2+H]^+$ = 488.2079, found = 488.2091.

(*R*)-(2-Benzylpiperidin-1-yl)(3-(bis(4-fluorophenyl)(hydroxy)methyl)-1*H*-1,2,4-triazol-1-yl)methanone (**3**)

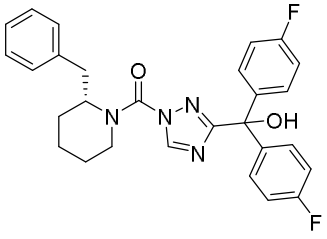

Synthesized according to General Procedure 1 from **21** (65 mg, 0.23 mmol). The title compound was obtained as a white solid (34.7 mg, 0.071 mmol, 35%). ^{1}H NMR (400 MHz, CD_3CN) δ 8.04 (bs, 1H), 7.35 (d, *J* = 6.6 Hz, 4H), 7.12 (s, 3H), 7.07 – 6.70 (m, 7H), 4.88 (s, 1H), 4.72 (s, 1H), 4.03 (d, *J* = 15.5 Hz, 1H), 3.23 (t, *J* = 13.1 Hz, 1H), 2.70 (s, 1H), 1.83 – 1.32 (m, 6H). HRMS: Calculated for $[C_{28}H_{26}F_2N_4O_2+H]^+$ = 488.2097, found = 488.2096.

(*R*)-(2-Benzylpiperidin-1-yl)(3-(bis(4-fluorophenyl)(hydroxy)methyl)-1*H*-pyrazol-1-yl)methanone (**4**)

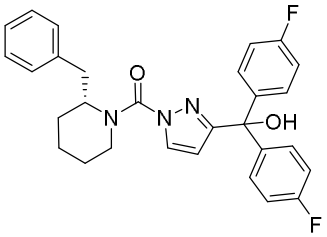

Synthesized according to General Procedure 1 from **25** (65 mg, 0.23 mmol). The title compound was obtained as a white solid (21 mg, 0.043 mmol, 21%). ^{1}H NMR (400 MHz, CD_3CN) δ 7.66 – 7.49 (m, 1H), 7.42 – 7.29 (m, 4H), 7.17 (dd, *J* = 5.1, 1.9 Hz, 3H), 7.13 – 6.92 (m, 6H), 6.22 (d, *J* = 2.6 Hz, 1H), 4.77 (s, 1H), 4.59 (s, 1H), 4.17 – 3.99 (m, 1H), 3.25 (td, *J* = 13.4, 3.0 Hz, 1H), 3.10 (dd, *J* = 13.5, 9.0 Hz, 1H), 2.83 – 2.68 (m, 1H), 1.88 – 1.21 (m, 6H). HRMS: Calculated for $[C_{29}H_{27}F_2N_3O_2+H]^+$ = 488.2144, found = 488.2140.

(*R*)-(2-Benzylpiperidin-1-yl)(4-(bis(4-fluorophenyl)(hydroxy)methyl)-1*H*-imidazol-1-yl)methanone (**5**)

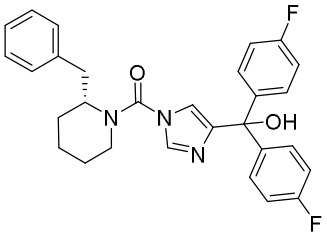

Synthesized according to General Procedure 1 from **29** (83 mg, 0.29 mmol). The title compound was obtained as a white solid (38 mg, 0.078 mmol, 27%). ^{1}H NMR (400 MHz, CD_3CN) δ 7.42 (s, 1H), 7.38 – 6.99 (m, 13H), 6.27 (s, 1H), 4.47 (s, 1H), 4.30 (qt, *J* = 7.1, 3.8 Hz, 1H), 3.81 (d, *J* = 13.7 Hz, 1H), 3.32 (td, *J* = 13.3, 2.9 Hz, 1H), 3.19 (dd, *J* = 13.7, 10.0 Hz, 1H), 2.78 (dd, *J* = 13.7, 5.5 Hz, 1H), 1.92 – 1.63 (m, 6H).
HRMS: Calculated for $[C_{29}H_{27}F_2N_3O_2+H]^+$ = 488.2144, found = 488.2142.

(4-([1,1'-Biphenyl]-4-yl)-1*H*-1,2,3-triazol-1-yl)(2-benzylpiperidin-1-yl)methanone (KT109)

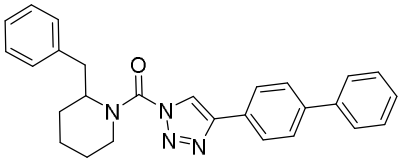

Synthesized according to General Procedure 1 from **30** (2.31 g, 10.4 mmol). The *N*1-isomer was isolated as first eluting isomer (621 mg, 1.47 mmol, 14%). ^{1}H NMR (400 MHz, $CDCl_3$) δ 7.87 (s, 2H), 7.75 – 7.60 (m, 4H), 7.53 – 7.35 (m, 4H), 7.24 (d, *J* = 15.7 Hz, 6H), 4.86 (s, 1H), 4.37 (d, *J* = 13.5 Hz, 1H), 3.31 (d, *J* = 52.1 Hz, 2H), 2.70 (s, 1H), 2.11 – 1.62 (m, 6H).

HRMS: Calculated for $[C_{27}H_{26}N_4O + H]^+$ = 423.2179, found = 423.2183.

Supplementary Figures

```
[task]
data = progress | task = fit

[mechanism]
E + S ---> E + P : kprod
                              E + I <==> E.I : kon* koff
E.I ---> E-I : kinact
E ---> E* : kdeg

[constants] | kprod = 4.7 ?, kon* = 100000, koff = 400 ?, kinact = 1 ?, kdeg = 0.027 ?

[concentrations] | E = 0.001 ? (0.0005 .. 0.005), S = 600

[responses] | P = 0.001735

[data]
directory ../Input
sheet 2018-07-10_filename_001.txt
column 2 | offset = auto ? (-0.2 .. +0.2) | conc I = 0
column 7 | offset = auto ? (-0.2 .. +0.2) | conc I = 0.008
column 8 | offset = auto ? (-0.2 .. +0.2) | conc I = 0.004
column 9 | offset = auto ? (-0.2 .. +0.2) | conc I = 0.002
column 10 | offset = auto ? (-0.2 .. +0.2) | conc I = 0.001
column 11 | offset = auto ? (-0.2 .. +0.2) | conc I = 0.0005
column 12 | offset = auto ? (-0.2 .. +0.2) | conc I = 0.00025
column 13 | offset = auto ? (-0.2 .. +0.2) | conc I = 0.000125

[output]
directory ../Output/2018-07-10_filename_001/2018-07-10_filename_001_compound/

[settings] | {Constraints} |

[end]
```

Figure S4.1 | Example DynaFit script. All concentrations are in µM units, rate constants are given in min^{-1} (k_{off}, k_{inact} and k_{deg}) or $M^{-1}min^{-1}$ (k_{prod} and k_{on})

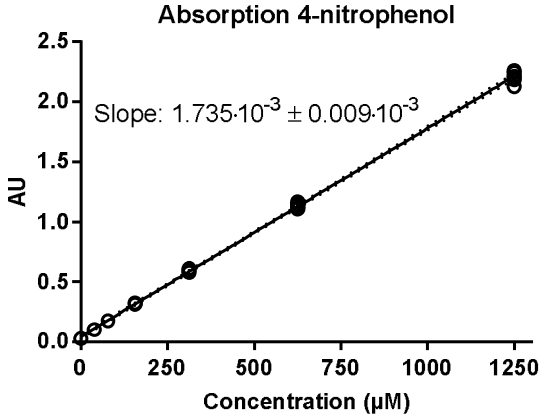

Figure S4.2 | Absorption of 4-nitrophenol. Linear curve fit of absorbance measured for a concentration of 4-nitrophenol in the assay buffer. 6 repetitions are given for each condition. Dashed lines denote 95% confidence interval. Slope value is given ± standard deviation.

References

1. Zhao, Z. & Bourne, P. E. Progress with covalent small-molecule kinase inhibitors. *Drug Discov. Today* **23**, 727–735 (2018).
2. Singh, J., Petter, R. C., Baillie, T. a & Whitty, A. The resurgence of covalent drugs. *Nat. Rev. Drug Discov.* **10**, 307–317 (2011).
3. Keith, J. M. *et al.* Preclinical Characterization of the FAAH Inhibitor JNJ-42165279. *ACS Med. Chem. Lett.* **6**, 1204–1208 (2015).
4. Postnov, A. *et al.* Fatty Acid Amide Hydrolase Inhibition by JNJ-42165279: A Multiple-Ascending Dose and a Positron Emission Tomography Study in Healthy Volunteers. *Clin. Transl. Sci.* **11**, 397–404 (2018).
5. Johnson, D. S. *et al.* Discovery of PF-04457845: A Highly Potent, Orally Bioavailable, and Selective Urea FAAH Inhibitor. *ACS Med. Chem. Lett.* **2**, 91–96 (2011).
6. Huggins, J. P., Smart, T. S., Langman, S., Taylor, L. & Young, T. An efficient randomised, placebo-controlled clinical trial with the irreversible fatty acid amide hydrolase-1 inhibitor PF-04457845, which modulates endocannabinoids but fails to induce effective analgesia in patients with pain due to osteoarthritis of th. *Pain* **153**, 1837–1846 (2012).
7. Cisar, J. S. *et al.* Identification of ABX-1431, a Selective Inhibitor of Monoacylglycerol Lipase and Clinical Candidate for Treatment of Neurological Disorders. *J. Med. Chem.* **61**, 9062–9084 (2018).
8. Fraser, I. *et al.* Preclinical characterization and first-in-human administration of a selective monoacylglycerol lipase inhibitor, ABX-1431. in *Front. Pharmacol. Conference Abstract: EUFEMED 2017* (2017). doi:10.3389/conf.fphar.2017.62.00011
9. Copeland, R. A. *Evaluation of enzyme inhibitors in drug discovery : a guide for medicinal chemists and pharmacologists*. (Wiley, 2013).
10. Schwartz, P. A. *et al.* Covalent EGFR inhibitor analysis reveals importance of reversible interactions to potency and mechanisms of drug resistance. *Proc. Natl. Acad. Sci.* **111**, 173–178 (2014).
11. Aaltonen, N. *et al.* Piperazine and Piperidine Triazole Ureas as Ultrapotent and Highly Selective Inhibitors of Monoacylglycerol Lipase. *Chem. Biol.* **20**, 379–390 (2013).
12. van Esbroeck, A. C. M. *et al.* Activity-based protein profiling reveals off-target proteins of the FAAH inhibitor BIA 10-2474. *Science* **356**, 1084–1087 (2017).
13. Kerbrat, A. *et al.* Acute Neurologic Disorder from an Inhibitor of Fatty Acid Amide Hydrolase. *N. Engl. J. Med.* **375**, 1717–1725 (2016).
14. Miyahisa, I., Sameshima, T. & Hixon, M. S. Rapid Determination of the Specificity Constant of Irreversible Inhibitors (k inact / K I) by Means of an Endpoint Competition Assay. *Angew. Chemie Int. Ed.* **54**, 14099–14102 (2015).
15. Ahn, K. *et al.* Mechanistic and Pharmacological Characterization of PF-04457845: A Highly Potent and Selective Fatty Acid Amide Hydrolase Inhibitor That Reduces Inflammatory and Noninflammatory Pain. *J. Pharmacol. Exp. Ther.* **338**, 114–124 (2011).
16. Strelow, J. M. A Perspective on the Kinetics of Covalent and Irreversible Inhibition. *SLAS Discov. Adv. Life Sci. R&D* **22**, 3–20 (2017).
17. Bisogno, T. *et al.* Cloning of the first sn1-DAG lipases points to the spatial and temporal regulation of endocannabinoid signaling in the brain. *J. Cell Biol.* **163**, 463–468 (2003).
18. Janssen, F. J. & van der Stelt, M. Inhibitors of diacylglycerol lipases in neurodegenerative and metabolic disorders. *Bioorg. Med. Chem. Lett.* **26**, 3831–3837 (2016).
19. Baggelaar, M. P., Maccarrone, M. & van der Stelt, M. 2-Arachidonoylglycerol: A signaling lipid with manifold actions in the brain. *Prog. Lipid Res.* **71**, 1–17 (2018).
20. Ogasawara, D. *et al.* Rapid and profound rewiring of brain lipid signaling networks by acute diacylglycerol lipase inhibition. *Proc. Natl. Acad. Sci.* **113**, 26–33 (2016).
21. Hsu, K.-L. *et al.* Discovery and Optimization of Piperidyl-1,2,3-Triazole Ureas as Potent, Selective, and in Vivo-Active Inhibitors of α/β-Hydrolase Domain Containing 6 (ABHD6). *J. Med. Chem.* **56**, 8270–8279 (2013).
22. Baggelaar, M. P. *et al.* Highly Selective, Reversible Inhibitor Identified by Comparative Chemoproteomics Modulates Diacylglycerol Lipase Activity in Neurons. *J. Am. Chem. Soc.* **137**, 8851–8857 (2015).
23. Adibekian, A. *et al. Optimization and characterization of a triazole urea inhibitor for alpha/beta hydrolase domain-containing protein 11 (ABHD11): anti-probe for LYPLA1/LYPLA2 dual inhibitor ML211*. *Probe Reports from the NIH Molecular Libraries Program* (National Center for Biotechnology Information (US), 2010).
24. Inloes, J. M. *et al.* The hereditary spastic paraplegia-related enzyme DDHD2 is a principal brain triglyceride lipase. *Proc. Natl. Acad. Sci.* **111**, 14924–14929 (2014).
25. Brindisi, M. *et al.* Development and Pharmacological Characterization of Selective Blockers of 2-Arachidonoyl Glycerol Degradation with Efficacy in Rodent Models of Multiple Sclerosis and Pain. *J. Med. Chem.* **59**, 2612–2632 (2016).
26. Hsu, K.-L. *et al.* Development and Optimization of Piperidyl-1,2,3-Triazole Ureas as Selective Chemical Probes of Endocannabinoid Biosynthesis. *J. Med. Chem.* **56**, 8257–8269 (2013).

27. Deng, H. *et al.* Triazole Ureas Act as Diacylglycerol Lipase Inhibitors and Prevent Fasting-Induced Refeeding. *J. Med. Chem.* **60**, 428–440 (2017).
28. Clayden, J., Greeves, N. & Warren, S. Nucleophilic substitution at the carbonyl group. in *Organic Chemistry* 197–221 (2012).
29. Blais, M.-J., Enea, O. & Berthon, G. Relations structure-réactivité grandeurs thermodynamiques de protonation d'h'et'erocycles saturés et non saturés. *Thermochim. Acta* **20**, 335–345 (1977).
30. Catalan, J. *et al.* Basicity and acidity of azoles: the annelation effect in azoles. *J. Am. Chem. Soc.* **110**, 4105–4111 (1988).
31. Hansen, L. D., West, B. D., Baca, E. J. & Blank, C. L. Thermodynamics of proton ionization from some substituted 1,2,3-triazoles in dilute aqueous solution. *J. Am. Chem. Soc.* **90**, 6588–6592 (1968).
32. Baggelaar, M. P. *et al.* Development of an Activity-Based Probe and In Silico Design Reveal Highly Selective Inhibitors for Diacylglycerol Lipase-α in Brain. *Angew. Chemie Int. Ed.* **52**, 12081–12085 (2013).
33. Zhao, K.-Y. & Tsou, C.-L. Kinetics of substrate reaction during irreversible modification of enzyme activity where the modifier is not in great excess of the enzyme. *J. Theor. Biol.* **157**, 505–521 (1992).
34. Maurer, T. S. & Fung, H.-L. Comparison of methods for analyzing kinetic data from mechanism-based enzyme inactivation: Application to nitric oxide synthase. *AAPS PharmSci* **2**, 68–77 (2000).
35. Krippendorff, B.-F., Neuhaus, R., Lienau, P., Reichel, A. & Huisinga, W. Mechanism-based inhibition: deriving K(I) and k(inact) directly from time-dependent IC(50) values. *J. Biomol. Screen.* **14**, 913–23 (2009).
36. Kuzmič, P. Program DYNAFIT for the Analysis of Enzyme Kinetic Data: Application to HIV Proteinase. *Anal. Biochem.* **237**, 260–273 (1996).
37. Kuzmič, P. DynaFit–a software package for enzymology. *Methods Enzymol.* **467**, 247–80 (2009).
38. Hsu, K. *et al.* DAGLβ inhibition perturbs a lipid network involved in macrophage inflammatory responses. *Nat. Chem. Biol.* **8**, 999–1007 (2012).
39. Mileni, M. *et al.* Structure-guided inhibitor design for human FAAH by interspecies active site conversion. *Proc. Natl. Acad. Sci.* **105**, 12820–12824 (2008).
40. Edwards, P. D. *et al.* Design, synthesis, and kinetic evaluation of a unique class of elastase inhibitors, the peptidyl α-ketobenzoxazoles, and the x-ray crystal structure of the covalent complex between porcine pancreatic elastase and Ac-Ala-Pro-Val-2-benzoxazole. *J. Am. Chem. Soc.* **114**, 1854–1863 (1992).
41. Janssen, F. J. *et al.* Comprehensive Analysis of Structure–Activity Relationships of α-Ketoheterocycles as sn-1-Diacylglycerol Lipase α Inhibitors. *J. Med. Chem.* **58**, 9742–9753 (2015).
42. Gottlieb, H. E., Kotlyar, V. & Nudelman, A. NMR Chemical Shifts of Common Laboratory Solvents as Trace Impurities. *J. Org. Chem.* **62**, 7512–7515 (1997).
43. Blacker, A. J. *et al.* Convenient Method for Synthesis of N-Protected α-Amino Epoxides: Key Intermediates for HIV Protease Inhibitors. *Org. Process Res. Dev.* **15**, 331–338 (2011).
44. Taherpour, A. A. & Kheradmand, K. One-pot microwave-assisted solvent free synthesis of simple alkyl 1,2,3-triazole-4-carboxylates by using trimethylsilyl azide. *J. Heterocycl. Chem.* **46**, 131–133 (2009).
45. Fatin-Rouge, N. *et al.* Lanthanide Podates with Programmed Intermolecular Interactions: Luminescence Enhancement through Association with Cyclodextrins and Unusually Large Relaxivity of the Gadolinium Self-Aggregates. *J. Am. Chem. Soc.* **122**, 10810–10820 (2000).